Atomic structure and polarization line shift in dense and hot plasmas

Hoe Nguyen, Michel Koenig, Djamel Benredjem, Monique Caby, and Gérard Coulaud
Département de Recherches Physiques, Laboratoire Spectronomie des Gaz et des Plasmas, Université Pierre et Marie Curie, 4 place Jussieu, 75230 Paris Cedex 05, France
and Groupement de Recherches Coordonnées de l'Interaction Laser-Matière du Centre National de Recherche Scientifique, Ecole Polytechnique, 91120 Palaiseau, France
(Received 27 December 1984; revised manuscript received 16 July 1985)

A model of a confined atom in a self-consistent field has been developed to describe the high-density effects on atomic bound states in plasmas. Numerical values, asymptotic behaviors, and scaling laws are given for energy levels and spectral line shifts. Concurrently, a suitable quantum-mechanical impact calculation has been performed to obtain linewidths and line shifts. For a typical electron temperature and density of laser plasma, it has been shown that line shifts given by the two approaches are in agreement within 10%.

I. INTRODUCTION

The study of atomic systems embedded in a finite-temperature and -density environment is one of the major subjects of current research in astrophysics and in condensed-matter and plasma physics. In recent years, renewed interest has been principally stimulated by inertial-confinement research, where it occurs both in spectroscopic diagnostic methods and in target dynamics or the plasma equation of state. Indeed, experiments with high-power laser beams produce plasmas having an electron density and temperature as high as 10^{24} cm^{-3} and 1000 eV, respectively. It is difficult to diagnose such plasmas because they are neither homogeneous nor static. However, modern diagnostic technology provides space and time resolution of a few micrometers and a hundred picoseconds, respectively. Therefore, it is now possible to obtain space- and/or time-resolved x-ray line spectra.

Several theoretical papers[1-5] concerning line-broadening aspects of such data are already available. However, for very-high-density plasmas which are strongly coupled with the radiating systems, a more detailed understanding of experimental data is essential and necessitates improvement of fundamental theory of atomic structure. Among the basic and controversial subjects we must mention the so-called "plasma polarization shift,"[6] which has to be considered in spectroscopic diagnostics and design of future x-ray lasers.[7] Up to now, most of the theoretical models of line shift are based on linearized Debye-Hückel theory and are not satisfactory for at least two reasons. Firstly, the linearization is valid at large distance from the ion and not close to the nucleus where the model is applied. Secondly, this *a priori* electrostatic potential ignores completely the reaction of plasma electrons to the presence of bound electrons. Some recent works have taken into account this reaction by solving the nonlinear Poisson equation. Unfortunately the obtained ion effects are rather doubtful because they imply (a) first, the Boltzmann distribution which is erroneous for strong ion coupling[8] and (b) second, the polarization of the ion component which has a correlation time much longer than the lifetime of excited atomic states.

In a suitable atomic model we note the following: (i) All the bound states are confined inside the ion sphere with radius $R_0=(4\pi N_i/3)^{-1/3}$ where N_i denotes the ion density. (ii) Only plasma components with correlation time smaller than the effective atomic lifetime can be polarized.

In high-density and low-temperature plasmas, such as in the solid phase, the ions are packed together tightly and each ion occupies an equal volume. Indeed, Monte Carlo simulations[9] for strongly coupled plasmas show that the ion radial distribution function is negligibly small at short distances r and increases sharply to unity for $r\simeq R_0$. So, atomic states with orbit radius $r_n > R_0$ actually belong to the continuum. At higher temperatures (or lower densities), the ions are more randomly distributed and there is a large fluctuation of the volume occupied by different ions. Here the linearized Debye theory is valid and lays down that interactions can occur over the Debye sphere and imply a large number of ions. Nevertheless, it is easy to show that the assertion (i) holds still true here. Among the main causes of this we ought to mention the fluctuating ion microfield $F_0\simeq Ze/R_0^2$ which is to be compared with the ionizing critical field[3,10] $F_c\simeq E_n^2/e^3Z$ where $E_n=-Ze^2/r_n$ denotes the atomic binding energy. We have to consider also the electron pressure ionization.[11] Indeed, taking into account the electric neutrality condition $N_e=ZN_i$, the number of free electrons compressed inside an atom is $\Delta Z\simeq 4\pi N_e r_n^3/3=Z(r_n/R_0)^3$ and corresponds to the complete screening of the nuclear charge for all atomic orbit radii $r_n \geqq R_0$.

Concerning the assertion (ii) relative to time scaling, the effective atomic lifetime τ_n can be estimated by the inverse of the corresponding electron-produced linewidth. As given by Eq. (30) in Sec. III, τ_n is of the order of 10^{-16} sec. The electron correlation time τ_e (equal to the inverse of the plasma frequency) is about 10^{-17} sec while the ion correlation time is $\tau_i\simeq(M_i/m)^{1/2}\tau_e\simeq 60\sqrt{Z}\,\tau_e$ where M_i and m are the ion and electron mass, respectively. Then, we have generally the double condition

$$\tau_e \ll \tau_n \ll \tau_i \ . \tag{1}$$

The condition $\tau_n \ll \tau_i$ means that the lifetime of atomic states is too short for the ion component to be effectively polarized. Its effect on spectral lines could be treated separately via the quasistatic Stark effect[1,2] or the adiabatic approximation including ion dynamic effects.[12]

The condition $\tau_e \ll \tau_n$ in Eq. (1) ensures that the atomic state exists through several oscillation periods of free electrons. Therefore, the time average for atomic properties and its equivalent ensemble average are meaningful. The former will be performed in Sec. III by means of a quantum-mechanical electron-impact theory[13] while the latter will be obtained in Sec. II by using a self-consistent-field method for confined atoms.[14]

II. SELF-CONSISTENT-FIELD METHOD FOR CONFINED ATOMS

In pursuance of the previous remarks on the localization of bound states and on the time scaling in polarization effects, we are finally left with the following atomic model: the nuclear charge $Z_E e$ is at the center of a spherical cavity with a radius $R_0=[3(Z_E-k)/4\pi N_e]^{1/3}$ where k is the number of bound electrons. To focus attention we shall consider only the case $k=1$, i.e., hydrogenlike atomic systems. Inside the ion sphere there are sufficient electrons to give an overall electrical neutrality. Outside the ion sphere the plasma is replaced by neutralizing uniform distributions due to electrons and ions, which lead to a constant electrostatic potential conventionally taken to be zero. On the average, an electron moves through an electrostatic potential $\phi(r)$ defined by the Poisson equation with the central point charge Z_E, the number density of free electrons $\rho_e(r)$, and that of the bound electron $\rho_b(r)$. Generally plasma temperatures are much higher than the Fermi temperature:

$$kT > kT_F=(3\pi^2 a_0^3 N_e)^{2/3}\ (\mathrm{Ry}) =36.5[10^{-24}N_e\ (\mathrm{cm}^{-3})]^{2/3}\ (\mathrm{eV})\ , \tag{2}$$

so that Maxwell-Boltzmann statistics can be used. Therefore, in terms of the energies $E(nl)$ and the radial wave functions $R_{nl}(r)$ of the bound states, $\rho_b(r)$ can be written as

$$\rho_b(r)=\frac{1}{4\pi}\left[\sum_{n,l} b(nl)R_{nl}^2(r)\right]\left[\sum_{n,l} b(nl)\right]^{-1}\ , \tag{3}$$

where

$$b(nl)=(2l+1)\exp\{-[E(nl)-E(10)]/kT\}\ . \tag{4}$$

Likewise, the number density of free electrons is given by

$$\rho_e(r)=\rho_e(R_0)\frac{4}{\sqrt{\pi}} \times\int_{p_0}^{\infty}\frac{p^2}{(2mkT)^{3/2}}dp \times\exp\left[-\frac{1}{kT}\left[\frac{p^2}{2m}-e\phi(r)+Q(r)\right]\right]\ , \tag{5}$$

where

$$p_0=p_0(r)=\{2m[e\phi(r)-Q(r)]\}^{1/2} \tag{6}$$

and the momentum condition $p\geqq p_0$ ensures that the kinetic energy of free electrons is larger than the (negative) potential energy. In Eq. (5), Q denotes the quantum-mechanical correction to the energy consisting of three terms; the exchange energy Q_{ex}, the correlation energy Q_{corr}, and the gradient correction energy Q_{gr}. The first two, Q_{ex} and Q_{corr},[15,16] result from antisymmetrizing the electron wave function. Physically, they prevent two electrons from occupying the same quantum state in accordance with the Pauli exclusion principle. The gradient correction energy Q_{gr} takes into account the Heisenberg space-momentum uncertainty relation and prevents the formation of a large electron-density gradient.[17,18]

Instead of $Q_{\mathrm{ex}}(r)+Q_{\mathrm{corr}}(r)+Q_{\mathrm{gr}}(r)$ we use, in fact,

$$Q(r)=Q_{\mathrm{ex}}(r)+Q_{\mathrm{corr}}(r)+Q_{\mathrm{gr}}(r) -[Q_{\mathrm{ex}}(R_0)+Q_{\mathrm{corr}}(R_0)+Q_{\mathrm{gr}}(R_0)]\ , \tag{7}$$

so that the quantum-mechanical correction in Eq. (5) is zero on the ion sphere. In accordance with the atomic model described in Sec. I, the hydrogenlike ion-sphere radius is

$$R_0=[3(Z_E-1)/4\pi N_e]^{1/3}\ , \tag{8}$$

where N_e is the volume-averaged electron density, called electron density for short, and considered together with T as input data in our problem.

With regard to the electrostatic potential we assume the following boundary conditions;

$$\phi(r)=\phi(R_0)=0 \quad \text{for } r\geqq R_0 \tag{9}$$

and

$$\left[\frac{d\phi(r)}{dr}\right]_{r=R_0}=0\ . \tag{10}$$

For $r<R_0$ the suitable solution of the Poisson equation takes then the form

$$\phi(r)=Z_E e/r+\phi_e(r)+\phi_b(r)\ , \tag{11}$$

where the first term is the contribution of the central charge $Z_E e$ while those of free and bound electrons are related to number densities according to

$$\phi_{e,b}=-4\pi e\left[\frac{1}{r}\int_0^r r'+\int_r^{R_0}\right]r'dr'\rho_{e,b}(r')\ . \tag{12}$$

The above boundary conditions on the solution of the Poisson equation call for the following two remarks.

Firstly, Eqs. (7) and (9) show that the potential energy vanishes on the ion sphere. Therefore, taking into account the normalization condition of the Maxwellian distribution function we find that the prefactor $\rho_e(R_0)$ on the right-side member of Eq. (5) has really the meaning of the boundary electron density. As a result of the plasma polarization, the latter is generally smaller than the volume-averaged electron density:

$$N_e=\frac{3}{R_0^3}\int_0^{R_0} r^2 dr\,\rho_e(r)\ . \tag{13}$$

Secondly, the condition, Eq. (10), also used for the Wigner-Seitz cell in solid-state physics, means that the radial electric field vanishes and no electron current takes place through the boundary surface. Taking into account Eqs. (11) and (12) we note that

$$E(R_0)=-\left[\frac{r}{r}\frac{d\phi(r)}{dr}\right]_{r=R_0}$$
$$=\frac{R_0 e}{R_0^3}\left[Z_E-4\pi\int_0^{R_0}r^2dr[\rho_e(r)+\rho_b(r)]\right]$$
$$=0\ .$$

Then, the confinement condition, Eq. (10), turns out to be the electrical neutrality condition for the whole atom including free and bound electrons

$$Z_E=4\pi\int_0^{R_0}r^2dr[\rho_e(r)+\rho_b(r)]=4\pi N_e R_0^3/3+1\ . \tag{14}$$

This is consistent with expressions defining the atom radius, Eq. (8), and the bound-electron number density, Eq. (3), where the normalization condition

$$\int_0^{R_0}r^2dr\,R_{nl}^2(r)=1$$

is assumed.[19]

Finally, to complete the description of the system, we have to consider the Schrödinger equation for the bound electron

$$\{-(\hbar^2/2m)[d^2/dr^2-l(l+1)/r^2]+V_a(r)-E(nl)\}[rR_{nl}(r)]=0\ , \tag{15}$$

where we assume the boundary condition[19]

$$R_{nl}(R_0)=0 \tag{16}$$

and introduce the effective atomic potential

$$V_a(r)=-e[Z_E e/r+\phi_e(r)]\ , \tag{17}$$

from which the self-energy of the bound electron $-e\phi_b(r)$ is excluded, as it should. With regard to Eqs. (5), (12), and (13), we note that $\phi_e(r)$ tends to vanish with decreasing N_e and, consequently, Eq. (15) reduces to the unperturbed Schrödinger equation.

When the temperature is high enough so that the kinetic energy overcomes completely the potential energy, Eq. (5) shows that the number density of free electrons is indeed spatially independent. Thus, according to Eq. (12), the atomic potential reduces to the following uniform electron-gas model (UEGM):

$$V_a^{\mathrm{UEGM}}(r)=-e[Z_E e/r+\lim_{T\to\infty}\phi_e(r)]$$
$$=-e^2\{-Z_E/r+2\pi N_e R_0^2[1-\tfrac{1}{3}(r/R_0)^2]\}\ . \tag{18}$$

In the right-hand side of Eq. (18), the first term in square brackets corresponds to the continuum lowering[20] while the second one gives rise to spectral line shifts. In the low-density limit, justifying the first-order perturbation theory, this second term can be expressed as

$$\Delta E(nl)\simeq-\frac{2\pi e^2N_e}{3}\langle nl\,|\,r^2\,|\,nl\rangle$$
$$=-\frac{\pi e^2N_e a_0^2}{3Z_E^2}n^2[5n^2+1-3l(l+1)]\ . \tag{19}$$

For any given N_e and T, in order to obtain fundamental parameters of the plasma (local electron density, electrostatic potential) and those of atomic bound states (energy levels, wave functions, occupation numbers, . . .), Eqs. (3), (5), (11), (12), and (15) should be solved self-consistently with the confinement conditions Eqs. (8), (9), (14), and (16).

The starting point consists in solving numerically Eq. (15) where the interaction potential $V_a(r)$ is initially replaced by its high-temperature limit V_a^{UEGM}, Eq. (18). This leads to atomic data and in particular to the electrostatic potential due to bound states $\phi_b(r)$, Eq. (12). First, we keep the latter unchanged and find self-consistent values for $\rho_e(R_0)$, $\rho_e(r)$, and $\phi_e(r)$ by considering together Eqs. (5), (9), (11), (12), and (14). This procedure requires up to four iterations. Then the new form of $\phi_e(r)$ is introduced in Eq. (15), the numerical solution of which constitutes a starting point for the following sequence of iterations. Generally, the first two sequences already yield self-consistent values of atomic data. Some more are really necessary only for extreme cases with low temperatures, high electron densities and high principal quantum numbers.

Figure 1 represents typical self-consistent values for the most interesting plasma and atomic parameters. Curve (a) shows that the number density of free electrons increases rapidly when r decreases towards the orbit-radius

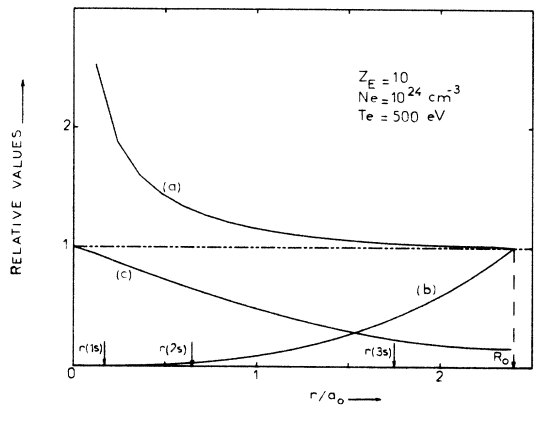

FIG. 1. Self-consistent values for a: free-electron density relative to that at the boundary surface, $\rho_e(r)/\rho_e(R_0)$; b: relative number of free electrons compressed inside the radius r, $4\pi\int_0^r r'^2dr'\rho_e(r')/(Z_E-1)$; c: effective atomic potential relative to the unperturbed Coulomb potential, $rV_a(r)/e^2Z_E$. For comparison purposes, the orbit radius values $r(nl)=\langle nl\,|\,r^2\,|\,nl\rangle^{1/2}$ are marked by means of arrows along the r axis.

TABLE I. Ne X energy levels $E(nl)$ (in Ry) calculated for a given temperature $T=500$ eV and various volume-averaged electron densities N_e. As shown in the second line we note that the boundary electron density $\rho_e(R_0)$ is appreciably smaller than the volume-averaged density.

N_e (cm^{-3})	6×10^{22}	1×10^{23}	3×10^{23}	6×10^{23}	1×10^{24}	3×10^{24}	6×10^{24}
$\rho_e(R_0)/N_e$	0.9822	0.9794	0.9723	0.9669	0.9620	0.9510	0.9421
$-E(1s)$	95.523	94.666	92.218	90.110	88.188	82.706	77.980
$-E(2s)$	20.538	19.700	17.336	15.348	13.582	8.863	5.312
$-E(2p)$	20.541	19.696	17.306	15.283	13.474	8.549	4.721
$-E(3s)$	6.736	5.951	3.849	2.280	1.065		
$-E(3p)$	6.728	5.932	3.790	2.162	0.972		
$-E(3d)$	6.702	5.890	3.666	1.910	0.606		
$-E(4s)$	2.075	1.427					
$-E(4p)$	2.056	1.394					
$-E(4d)$	2.014	1.324					
$-E(4f)$	1.952	1.217					

values of fundamental and first excited states. Therefore, the latter can hardly be treated by means of the uniform electron-gas approximation. As shown by curves (b) and (c), highly excited states ($3s$ state given in Fig. 1) are only weakly bound because of the large number of free electrons compressed inside their orbit and the significant reduction of the effective atomic potential at their location.

Table I presents the energy levels for the Ne X bound states existing in plasmas with $T=500$ eV and various N_e. For increasing N_e we note the following two points. (i) The number of bound states decreases rapidly. In fact, no bound state with $n=4$ and 3 exists when the volume-averaged density N_e goes beyond 10^{23} and 10^{24} cm^{-3}, respectively. (ii) All the energy levels move more and more towards the continuum. Besides, the energy shift $E(nl)-E^0(nl)=[E(nl)+100/n^2)]$ (Ry) increases with increasing orbital quantum number l and decreasing principal quantum number n. The latter fact provides for a red line shift which will be discussed in detail in Secs. III and IV.

Table II gives the same parameters as in Table I but with a fixed density $N_e=10^{24}$ cm^{-3} and various temperatures. The values at the infinite temperature limit (last line in Table II) have been obtained by solving numerically Eq. (15) with the effective atomic potential $V_a(r)$ replaced by the V_a^{UEGM} of Eq. (18). The numerical values given in the three right-hand-side columns show that the energy levels become deeper and deeper as the temperature increases. Physically, this can be explained by noting that the lower the temperature, the more efficient is the nuclear Coulomb attraction and, consequently, the larger is the fractional number of free electrons compressed inside an atomic orbit. As a result, the corresponding energy level tends towards the continuum from its deepest value given by the UEGM. Also, comparing the transition energy $E(2p)-E(1s)$ of the Ne X Lyman-α line to the unperturbed one (75 Ry), we point out a red line shift which decreases with increasing T.

TABLE II. Ne X energy levels $E(nl)$ (in Ry) calculated for a given volume-averaged electron density $N_e=10^{24}$ cm^{-3} and various temperatures. We note that $E(nl)$ and $\rho_e(R_0)/N_e$ tend towards the corresponding UEGM values as the electron temperature increases.

kT_e (eV)	$\rho_e(R_0)/N_e$	$-E(1s)$	$-E(2s)$	$-E(2p)$
100	0.8939	86.798	12.434	12.268
200	0.9292	87.529	13.042	12.907
400	0.9550	88.078	13.492	13.379
600	0.9664	88.307	13.680	13.577
800	0.9729	88.436	13.784	13.687
1000	0.9772	88.521	13.853	13.760
1200	0.9801	88.582	13.903	13.812
1500	0.9833	88.643	13.952	13.864
∞	1.0000	88.946	14.189	14.116

As already mentioned in the comment on Eq. (13), the second line of Table I and the second column of Table II show that the boundary electron density $\rho_e(R_0)$ is smaller than the volume-averaged one N_e. This lowering of the boundary electron pressure increases when N_e increases with a fixed T or when T decreases with a fixed N_e. Again, the physical explanation based on balancing the kinetic and potential energy is valid here.

III. QUANTUM-MECHANICAL IMPACT THEORY FOR LINEWIDTH AND LINE SHIFT

In Sec. II we have dealt with a neutral "confined atom" which consists of a spherical cavity having the radius $R_0=[3(Z_E-1)/4\pi N_e]^{1/3}$ and enclosing a central point charge $Z_E e$ and the corresponding number Z_E of bound and free electrons. We have obtained various fundamental plasma and atomic parameters (local electron density, energy levels, and wave functions of bound electrons, etc.) except an essential one: the linewidth. To fill this gap, we shall consider a dynamical treatment of the total interaction between bound and free electrons. In addition to linewidths, we will obtain line shifts which must be compared to the previous self-consistent-field effects.

A. Basic equations

The general dynamical treatment, including non-Markovian effects such as the frequency dependence in

linewidth and line shift, is useful and numerically tractable only in some particular cases. In Sec. I we have already noted that the atomic lifetime τ_n is quite larger than the electron correlation (polarization) time τ_e. So, on an average it takes many collisions to produce an appreciable change in the wave functions of bound states. This is just the basic assumption which underlies the quantum-mechanical impact theory of pressure broadening. Following Baranger,[21] we can write the line shape for a group of overlapping radiative transitions $a\rightarrow\alpha$, $b\rightarrow\beta$, . . . , as follows:

$$I(\omega)=-\frac{\hbar}{\pi}\mathrm{Im}\sum_{a,b,\alpha,\beta}\langle\langle a\alpha^* \mid \Delta \mid b\beta^*\rangle\rangle\left\langle\left\langle b\beta^* \left| \frac{1}{\hbar\omega-(H_{Ai}-H_{Af}^*+\mathscr{K})} \right| a\alpha^*\right\rangle\right\rangle\rho_a \ , \tag{20}$$

where we have assumed that the density matrix is diagonal with respect to initial atomic states; Δ is the emission dipole in the doubled-atom description:

$$\langle\langle a\alpha^* \mid \Delta \mid b\beta^*\rangle\rangle=\langle a \mid \mathbf{d} \mid \alpha\rangle\langle\beta \mid \mathbf{d} \mid b\rangle \ .$$

H_{Ai} and H_{Af} are atomic Hamiltonians acting only on initial states $a,b,\ldots$, and final states $\alpha,\beta,\ldots$, respectively. In Eq. (20) $\mathscr{K}$ is the constant effective interaction accounting for the time-dependent interaction between free electrons and the ionic radiator of interest.

$\mathscr{K}$ has been conveniently expressed in terms of coupled representation T matrix elements in the literature [see, for example, Eqs. (205) and (206) of Ref. 6]. For the particular case of the Lyman series ($n_f=1, l_f=0$) we have

$$\langle\langle n_i l_i;n_f 0 \mid \mathscr{K} \mid n_i l_i;n_f 0\rangle\rangle=-\frac{i\pi N_e\hbar^3}{m^2}\left\langle\frac{1}{v(2l_i+1)}\sum_{L_i,l}(2L_i+1)[T_{L_i}(\nu_i,\nu_i)+T_l^+(\nu_f,\nu_f)-T_l^+(\nu_f,\nu_f)T_{L_i}(\nu_i,\nu_i)]\right\rangle_v \ , \tag{21}$$

where $\langle\ \rangle_v$ denotes the average over colliding electron velocity v. The T matrix elements are

$$T_{L_a}(\nu_a,\nu_a')=\langle n_a v;l_a l L_a \mid T \mid n_a' v;l_a' l' L_a\rangle \ , \tag{22}$$

with $a=i$ or f. They are to be evaluated without long-range Coulomb effects.[22]

Although the formal theory has been developed with the colliding electron distinguished from the bound electron, we recall the physical possibility for the former to remain inside the radiator and for the latter to be expelled in its place. To take this fact into account we will use instead of Eq. (22), the transition amplitudes $T_{L_a S}$ involving exchange effects and replace the factor $2L_i+1$ in Eq. (21) by $(2L_i+1)(2S+1)/4$.

B. Coulomb-Born-Oppenheimer approximation for highly charged radiators

In laser-produced plasmas the charge number Z_E of radiators is generally close to 10 or greater while the electron temperature is at least of the order of magnitude of several hundreds of electron volts. This is properly the validity condition for the Coulomb-Born-Oppenheimer (CBO) approximation[23] in the calculation of scattering data. Indeed, by using a_0/Z_E and $Z_E^2 e^2/a_0$ as units for length and energy, respectively, it is easy to see that the direct and exchange potentials in the perturber radial equation are equal to $1/Z_E$ multiplied by factors which depend on Z_E only through $\beta=(Z_E-1)/Z_E\simeq 1$ for $Z_E\gg 1$. Then, for sufficiently energetic colliding electrons, these potentials may be treated as small perturbations according to the CBO approximation which will be used here in its unitarized version by writing the transition matrix in the form

$$T^{\pm}=1-S^{\pm}=-2iR^{\pm}/(1-iR^{\pm}) \ , \tag{23}$$

where R^+ and R^- are real and symmetric reactance matrices corresponding to opposite ($S=0$) and parallel ($S=1$) electron spins, respectively. In the coupled representation their matrix elements can be written as

$$R_L^{\pm}(\nu_i,\nu_i')=-2\sum_{\lambda}[f_\lambda(l_i l L,l_i' l' L)D_\lambda(\nu_i,\nu_i') \pm(-1)^{l'+l_i'-L}f_\lambda(l l_i L,l_i' l' L) \times E_\lambda(\nu_i,\nu_i')] \ , \tag{24}$$

where f_λ denotes the angular factor for the 2^λ multipole and is expressed in terms of $3j$ and $6j$ symbols as

$$f_\lambda(l_i l L,l_i' l' L)=(-1)^{l_i+l_i'+L}\begin{Bmatrix} L & l_i & l \\ \lambda & l' & l_i' \end{Bmatrix}[(2l+1)(2l_i+1)(2l'+1)(2l_i'+1)]^{1/2}\begin{pmatrix} l' & \lambda & l \\ 0 & 0 & 0 \end{pmatrix}\begin{pmatrix} l_i' & \lambda & l_i \\ 0 & 0 & 0 \end{pmatrix} . \tag{25}$$

In Eq. (24) the direct integral D_λ and exchange integral E_λ involve radial perturber Coulomb wave functions $F_{\chi l}(\beta r)$ with $\chi=k/(Z_E-1)$, and radial atomic wave functions $P_{n_i l_i}(r)$.

We can express them as

$$D_\lambda(\nu_i,\nu_i')=\frac{1}{\beta Z_E}\int_0^\infty dr_2 F_{\chi l}(\beta r_2)F_{\chi' l'}(\beta r_2)\int_0^\infty dr\, P_{n_i l_i}(r_1)\left[\frac{r_<^\lambda}{r_>^{\lambda+1}}-\frac{\delta_{\lambda_0}}{r_2}\right]P_{n_i' l_i'}(r_1) \tag{26}$$

and

$$E_\lambda(\nu_i,\nu_i')=\frac{1}{\beta Z_E}\int_0^\infty dr_2 P_{n_i l_i}(r_2)F_{\chi' l'}(\beta r_2)\int_0^\infty dr\, F_{\chi l}(\beta r_1)\left[\frac{r_<^\lambda}{r_>^{\lambda+1}}-\frac{\delta_{\lambda_0}}{r_2}\right]P_{n_i' l_i'}(r_1) \tag{27}$$

where $r_<$ is the smallest and $r_>$ the largest of the reduced radii r_1 and r_2.

The set of Eqs. (21)–(27) will be used to evaluate the matrix elements occurring in the broadening of Lyman lines ($n_f=1$; $l_f=0$). Before doing this, it is interesting to compare cross sections presently obtained with the available ones coming from the close-coupling (CC) or distorted-wave (DW) method. The latter is characterized by the influence of diagonal potential matrix elements included in the perturber wave functions $F_{\chi l}$ while the former consists in solving coupled wave equations in the subspace generated by adequate pseudostates.

A numerical comparison between the CBO calculation and the CC (Ref. 24) one is illustrated by Table III (a) and III (b) for cross sections $\sigma(1s\rightarrow 2s)$ and $\sigma(1s\rightarrow 2p)$, respectively. We note that the agreement is quite satisfactory in the case of Ne X ion as target. However, in the case of the He II ion, the agreement is fairly acceptable only for sufficiently high incident energies. For completeness, we also give in Table III (a) and III (b) the Coulomb-Born (CB) values which were obtained by neglecting integrals E_λ in Eq. (24). By comparing them with the CBO values we note that the exchange effects can reach the order of magnitude of 15% and allow to improve appreciably the agreement with the corresponding CC values.[24]

In the line-broadening problem, more significant is the precision concerning elastic and inelastic cross sections which connect two excited states. Some of them are given in Table IV where we note that elastic cross sections differ slightly from the traditional ones owing to the monopolar interference effect of the ground state. For the most important bound-bound transitions, Table IV shows that our CBO values are in agreement with Griem, Blaha, and Kepple's DW results[1] (values in parentheses).

C. Linewidth and line shift

The linewidth and line shift are given, respectively, by the imaginary and real parts of the collision operator $\mathscr{K}$, Eq. (21). In fact, to ensure the continuity when colliding electron energies cross inelastic thresholds, the width has been expressed in terms of total cross sections for actual calculations. The latter have been performed as follows.

(i) For perturber orbital quantum number $l\leqq 20$, the cross sections connecting the ion bound states with principal quantum number $n\leqq 4$ have been obtained via the reactance matrix by using the CBO approximation (including exchange effects) to treat the monopole, dipole, quadrupole, and octopole interactions. The other bound-bound and bound-free cross sections are deduced from the Golden and Sampson[25] approximate formula where the ionization potential lowering effect is properly included. As already suggested in Ref. 1, total cross sections can be conveniently expressed in their equivalent semiclassical form:

$$\sigma(nl,E)=\frac{8\pi}{3}\left[\frac{e^2}{2a_0E}\right]\times\mathbf{r}\cdot\mathbf{r}\left[C(nl,E)+\frac{1}{2}\ln\frac{420}{L_{\min}(L_{\min}+1)}\right], \tag{28}$$

where $E=mv^2/2$ is the colliding electron energy, $L_{\min}$ is the minimum relative orbital quantum number corresponding to the impact parameter equal to the atomic orbit

$$L_{\min}(L_{\min}+1)=(mr_n v/\hbar)^2\simeq(n^2\hbar v/Z_E e^2)^2$$

and

$$\mathbf{r}\cdot\mathbf{r}=(3a_0 n/2Z_E)^2(n^2-l^2-l-1)$$

is an atomic operator introduced in previous second-order perturbation theories.[1,2,26] In Eq. (28), $C(nl,E)$, the so-called "strong-collision constant",[1,27,28] represents the contribution of collisions with $l<L_{\min}$ with quantum-mechanical corrections for other close collisions. Table IV shows that, at low energy, $C(nl,E)$ increases rapidly with E. Also, we note that the difference between our C values and those of Ref. 1 (given in large parentheses) comes mainly from transitions towards higher levels and the continuum which have been fully included in this work via the CBO approximation and partly neglected in Ref. 1.

(ii) The dipole interaction and semiclassical description are used to treat the weak collisions with $l\in[20,l_{\max}]$ where $l_{\max}$ is related to the maximum impact parameter $D_{\max}$ by

$$D_{\max}=\frac{\hbar}{mv}[l_{\max}(l_{\max}+1)]^{1/2}=v(\omega_p^2+\Delta\omega^2+\Delta\omega_S^2)^{-1/2}. \tag{29}$$

Here, the presence of the plasma frequency $\omega_p=(4\pi e N_e/m)^{1/2}$, of the frequency separation from the

TABLE III. Cross sections (a) $\sigma(1s\rightarrow 2s)$ and (b) $\sigma(1s\rightarrow 2p)$ (in units of $\pi a_0^2/Z_E^4$) deduced from our present Coulomb-Born (CB) or Coulomb-Born-Oppenheimer (CBO) calculation and those based on a close-coupling (CC) calculation (Ref. 23).

E	$Z=2$			$Z=10$		
(Z^2 Ry)	CC	CB	CBO	CC	CB	CBO
			(a) $\sigma(1s\rightarrow 2s)$			
0.7575	0.66	0.36	0.46	0.45	0.55	0.47
0.80	0.49	0.27	0.57	0.42	0.51	0.43
1	0.36	0.24	0.31	0.34	0.42	0.35
1.50	0.22	0.19	0.18	0.24	0.28	0.25
2		0.16	0.15		0.22	0.19
2.25	0.15	0.15	0.13	0.17	0.20	0.18
3	0.12	0.12	0.11	0.13	0.15	0.13
4		0.10	0.09		0.11	0.10
			(b) $\sigma(1s\rightarrow 2p)$			
0.7575	1.01	1.11	1.03	1.97	2.21	1.93
0.80	1.21	1.16	0.97	1.91	2.19	1.86
1	1.55	1.29	1.08	1.72	1.98	1.68
1.50	1.41	1.37	1.15	1.48	1.70	1.46
2		1.32	1.14		1.49	1.33
2.25	1.22	1.16	1.06	1.30	1.44	1.29
3	1.11	1.03	0.97	1.16	1.23	1.16
4		1.02	0.96		1.06	1.00

unperturbed line $\Delta\omega=\omega-\omega_0$ and of the frequency shift due to quasistatic perturbations $\Delta\omega_S$ allows for screening of electron fields, finite duration of the collisions and level splittings, respectively.

(iii) The thermal average has been performed by assuming the Maxwellian distribution for the electron velocity v and using the eight-point Gauss-Hermite integration.

Then the linewidth can be written as

TABLE IV. Cross sections $\sigma(np\rightarrow n')$ (in units of $\pi a_0^2/[E\ (\text{Ry})]$) calculated by CBO method for electron scattering on np levels of oxygen VIII. Only partial waves to $l=20$ are included. The difference of np and $1s$ scattering amplitudes was used to introduce interference effect in elastic cross sections. Griem *et al.*'s values (Ref. 1) are given in parentheses for comparison purpose. "Strong-collision constants" $C(nl,E)$ are defined from total cross sections $\sigma(nl)=\sum_{n'}\sigma(nl\rightarrow n')$ according to Eq. (28) in the text.

	$\sigma(2p\rightarrow n')$					
E (Ry)	$n'=2$	$n'=3$	$n'=4$	$n'\geq 5$ and continuum	$\sigma(2p)$	$C(2p,E)$
10	1.06	0.38	0	0	1.44	1.30
	(1.09)	(0.40)			(1.49)	(1.44)
20	1.01	0.49	0.10	0.12	1.72	2.40
	(1.03)	(0.51)			(1.54)	(2.19)
40	0.93	0.63	0.12	0.26	1.94	3.33
	(0.94)	(0.64)			(1.58)	(2.37)
	$\sigma(4p\rightarrow n')$					
E (Ry)	$n'=4$	$n'=2,3,5$	$n'\geq 6$ and continuum	$\sigma(4p)$	$C(4p,E)$	
10	26.9	4.6	2.6	34.1	0.60	
	(28.6)	(5.2)	(2.7)	(36.5)	(0.72)	
20	22.2	3.9	3.3	29.4	0.70	
	(23.2)	(4.3)	(2.7)	(30.2)	(0.74)	
40	16.9	2.8	3.9	23.6	0.75	
	(17.2)	(3.0)	(2.7)	(22.9)	(0.72)	

TABLE V. Temperature dependence of the "strong collision constant" $C(n,l,T)$ occurring in Lyman-α, -β, and -γ linewidths [see Eq. (30) in the text].

T (eV)/Z_E^2	$C(2s)$	$C(2p)$	$C(3s)$	$C(3p)$	$C(3d)$	$C(4s)$	$C(4p)$	$C(4d)$	$C(4f)$
1.00	−1.02	0.10	−0.43	−0.28	1.18	−0.18	−0.05	0.30	2.36
1.20	−0.95	0.22	−0.32	−0.15	1.40	−0.10	0.05	0.42	2.59
1.40	−0.85	0.36	−0.24	−0.05	1.61	−0.03	0.12	0.52	2.76
1.60	−0.75	0.51	−0.16	0.04	1.75	0.03	0.18	0.59	2.88
1.80	−0.66	0.64	−0.09	0.12	1.88	0.08	0.23	0.64	2.98
2.00	−0.58	0.77	−0.03	0.18	1.99	0.12	0.27	0.68	3.04
2.50	−0.40	1.04	0.08	0.32	2.23	0.19	0.32	0.72	3.10
3.00	−0.27	1.28	0.16	0.41	2.42	0.25	0.36	0.73	3.11
3.50	−0.15	1.48	0.21	0.48	2.60	0.30	0.40	0.78	3.18
4.00	−0.06	1.65	0.25	0.54	2.78	0.35	0.44	0.81	3.22
4.50	0.02	1.80	0.29	0.59	2.86	0.39	0.47	0.84	3.24
5.00	0.09	1.94	0.32	0.63	2.93	0.42	0.50	0.87	3.25
5.50	0.16	2.06	0.35	0.66	2.97	0.44	0.53	0.89	3.24
6.00	0.21	2.16	0.37	0.68	3.00	0.46	0.55	0.91	3.23
6.50	0.26	2.26	0.39	0.70	3.02	0.48	0.57	0.93	3.21
7.00	0.30	2.34	0.41	0.71	3.03	0.49	0.59	0.95	3.19
7.50	0.33	2.42	0.43	0.73	3.04	0.50	0.61	0.97	3.16
8.00	0.36	2.48	0.44	0.74	3.04	0.51	0.62	0.99	3.13
8.50	0.39	2.54	0.45	0.74	3.03	0.53	0.64	1.00	3.14
9.00	0.41	2.58	0.46	0.74	3.02	0.54	0.65	1.02	3.14
9.50	0.43	2.63	0.47	0.75	3.02	0.55	0.66	1.03	3.14
10.00	0.45	2.66	0.48	0.76	3.02	0.56	0.67	1.04	3.14
11.00	0.47	2.72	0.49	0.77	3.02	0.57	0.69	1.06	3.15
12.00	0.51	2.78	0.51	0.79	3.03	0.59	0.71	1.08	3.14
13.00	0.54	2.84	0.53	0.80	3.03	0.60	0.72	1.10	3.14
14.00	0.57	2.89	0.55	0.82	3.04	0.62	0.74	1.11	3.13
15.00	0.60	2.94	0.57	0.84	3.05	0.63	0.75	1.12	3.13
16.00	0.63	2.98	0.59	0.87	3.06	0.64	0.77	1.13	3.13
17.00	0.65	3.01	0.60	0.87	3.04	0.65	0.77	1.13	3.10
18.00	0.67	3.04	0.62	0.90	3.05	0.66	0.78	1.13	3.10
19.00	0.69	3.06	0.63	0.91	3.04	0.66	0.78	1.13	3.09
20.00	0.70	3.08	0.64	0.91	3.04	0.67	0.79	1.13	3.08

$$\mathrm{Im}\langle\langle nl,1s \mid \mathscr{H} \mid nl,1s \rangle\rangle = -N_e \langle v\sigma(nl,E)\rangle/2$$
$$= -\frac{4\pi N_e}{3}\left[\frac{2m}{\pi kT}\right]^{1/2}\frac{\hbar^3 \mathbf{r}\cdot\mathbf{r}}{m^2 a_0^2} \times \left[C(nl,T)+\tfrac{1}{2}\int_y^\infty \frac{e^{-x}dx}{x}\right], \quad (30)$$

where

$$y=\frac{1}{2}\left[\frac{\hbar n^2}{Z_E}\right]^2 \frac{(\omega_p^2+\Delta\omega_S^2+\Delta\omega^2)a_0}{e^2 kT}$$

and the thermally averaged strong collision constant $C(nl,T)$ is given in Table V. The calculation has been systematically performed for different n, l, T, and $Z_E \geqq 5$. The examination of numerical results shows the following.

(i) $C(nl,T)$ has a negligibly small dependence with respect to the charge number Z_E. Indeed, at low-temperature [T (eV)/$Z_E^2 \simeq 1$] $C(nl,T)$ increases by only 10% and 1% when Z_E varies from 5 to 10 and from 10 to 18, respectively. This Z_E dependence decreases rapidly for increasing temperature.

(ii) $C(nl,T)$ increases with T and tends towards a constant value at high temperature.

(iii) $C(nl,T)$ depends not only on the principal quantum number n but also strongly on the orbital quantum number l. Owing to the quasistatic field mixing effect, the line shape, Eq. (20), generally implies all the nl states regardless of the radiative selection rule. In this connection we note that the numerical values of $C(3d,T)$ and $C(4f,T)$ in Table V are particularly large. In using Eq. (30), we note that the semiclassical description of weak collisions implies the condition $l_{\max} \gtrsim 20$. This fact and considerations[1] relative to series limit, quasistatic splitting, finite duration of collisions and degeneracy suggest that the accuracy of the results is diminished more or less at high densities, except, say, for Lyman-α lines of $Z_E > 10$ elements.

As concerning the line shift, i.e., the real part of Eq. (21), we have to calculate directly the imaginary part of the elastic transition matrix elements in their unitarized form, Eq. (23). As previously we have taken into account the monopole, dipole, quadrupole, and octopole interactions. In fact, the numerical analysis shows that the monopole interaction plays a leading part in the red shift

TABLE VI. Temperature dependence of the Lyman-α, -β, and -γ line-shift factor $D(n,l,T)$ [see Eq. (46) in the text].

T (eV)/Z_E^2	$D(2s)$	$D(2p)$	$D(3s)$	$D(3p)$	$D(3d)$	$D(4s)$	$D(4p)$	$D(4d)$	$D(4f)$
1.00	11.75	8.93	42.41	38.08	29.18	104.63	98.83	86.17	67.25
1.20	10.82	8.20	39.57	35.47	27.06	98.09	92.64	80.65	62.78
1.40	10.11	7.64	37.36	33.44	25.42	93.53	88.28	76.70	59.44
1.60	9.54	7.20	35.64	31.85	24.12	90.12	85.00	73.68	56.86
1.80	9.08	6.83	34.24	30.56	23.06	87.31	82.29	71.21	54.74
2.00	8.69	6.53	33.06	29.48	22.18	84.93	80.01	69.12	52.96
2.50	7.94	5.93	30.77	27.38	20.46	80.25	75.52	65.06	49.53
3.00	7.39	5.50	29.08	25.83	19.22	76.88	72.29	62.13	47.08
3.50	6.97	5.17	27.78	24.64	18.27	74.48	69.97	60.02	45.26
4.00	6.63	4.91	26.73	23.68	17.51	72.58	68.15	58.35	43.82
4.50	6.36	4.70	25.93	22.95	16.91	71.03	66.65	56.98	42.65
5.00	6.13	4.52	25.26	22.33	16.41	69.72	65.39	55.84	41.67
5.50	5.94	4.37	24.69	21.81	15.98	68.59	64.30	54.86	40.83
6.00	5.77	4.24	24.19	21.35	15.62	67.61	63.36	54.02	40.11
6.50	5.63	4.12	23.75	20.95	15.29	66.73	62.52	53.27	39.47
7.00	5.50	4.02	23.35	20.59	15.01	65.93	61.76	52.60	38.89
7.50	5.39	3.93	23.01	20.28	14.75	65.20	61.07	51.99	38.38
8.00	5.28	3.85	22.70	20.01	14.53	64.56	60.46	51.46	37.93
8.50	5.19	3.78	22.43	19.76	14.33	64.00	59.92	50.98	37.54
9.00	5.11	3.71	22.19	19.54	14.15	63.48	59.42	50.55	37.19
9.50	5.03	3.65	21.96	19.33	13.98	62.99	58.96	50.14	36.87
10.00	4.96	3.60	21.74	19.13	13.83	62.51	58.51	49.76	36.57
11.00	4.83	3.50	21.36	18.79	13.56	61.64	57.70	49.07	36.05
12.00	4.72	3.41	21.04	18.49	13.33	60.91	57.02	48.49	35.60
13.00	4.63	3.34	20.74	18.23	13.12	60.26	56.41	47.98	35.21
14.00	4.56	3.28	20.41	17.94	12.90	59.50	55.70	47.37	34.75
15.00	4.49	3.23	20.21	17.75	12.75	58.98	55.19	46.95	34.43
16.00	4.42	3.18	20.07	17.61	12.64	58.49	54.72	46.55	34.14
17.00	4.24	3.05	19.96	17.50	12.53	58.02	54.27	46.19	33.88
18.00	4.19	3.01	19.85	17.39	12.44	57.57	53.85	45.84	33.63
19.00	4.15	2.97	19.70	17.26	12.34	57.11	53.43	45.51	33.40
20.00	4.11	2.94	19.55	17.14	12.24	56.65	53.03	45.19	33.19

of the Lyman lines. The higher orders of the multipolar expansion occur only in the higher members of the spectral series ($n \geq 3$) and lead to a slightly smaller red shift. It was found that the spectral line shift can be conveniently given in the form

$$\hbar\Delta\omega(nl \rightarrow 1s) = \mathrm{Re}\langle\langle nl,1s \mid \mathscr{H} \mid nl,1s \rangle\rangle = -\frac{10^{-22}N_e\ (\mathrm{cm}^{-3})}{Z_E^2} D(n,l,T)\ (\mathrm{eV}) \tag{31}$$

where, like the previous "strong collision constant," $C(n,l,T)$,$D(n,l,T)$ is nearly independent of Z_E for all $Z_E \geq 5$. As shown in Table VI, we note the following.

(i) $D(n,l,T)$ decreases smoothly with increasing l and varies approximately as the fourth power of n.

(ii) $D(n,l,T)$ decreases sharply when the temperature increases until the value $T \simeq 5Z_E^2$ eV. Beyond this temperature, $D(n,l,T)$ decreases smoothly and tends towards a finite limit $D(n,l,\infty)$ for extremely high temperatures.

For very-high-density plasmas, the two terms in large parentheses of Eq. (30) have the same order of magnitude. Then, comparing Eq. (30) with Table V to Eq. (31) with Table VI, we point out that the electron line shift can be much larger than the electron linewidth.

IV. COMPARISON OF RESULTS AND CONCLUDING REMARKS

Owing to the shortness of the electron correlation time τ_e compared to atomic lifetimes τ_n we have pointed out that atomic properties could be obtained from an ensemble average as well as from a time average. These two theoretical concepts have been developed by using, respectively, a model of a confined atom in self-consistent field (CASCF) in Sec. II and a quantum-mechanical impact theory (QMIT) in Sec. III. We will now proceed to compare them by examining the density and temperature dependence of the line shift which is one of the most important atomic parameters.

Figure 2 shows the density dependence of the Lyman-α line shift resulting from different theoretical models. The straight line (c) is obtained from the QMIT, Eq. (31), where the volume-averaged electron density is used. Indeed, this is not quite correct because electron collisions start at the atomic boundary surface. Then, using $\rho_e(R_0)$ instead of N_e, we obtain curve (a) which is to be com-

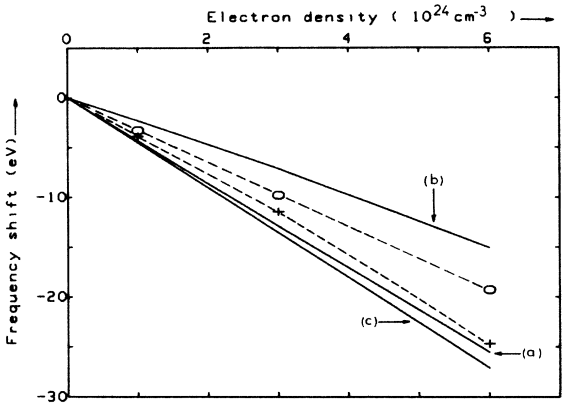

FIG. 2. Density dependence of the Ne X Lyman-α line shift calculated with $T=500$ eV. a: quantum-mechanical impact theory including the boundary depression effect. b: uniform electron-gas model. c: quantum-mechanical impact theory using the volume averaged electron density. + + +: confined atom in self-consistent field. OOO: results of Davis and Blaha (Ref. 15).

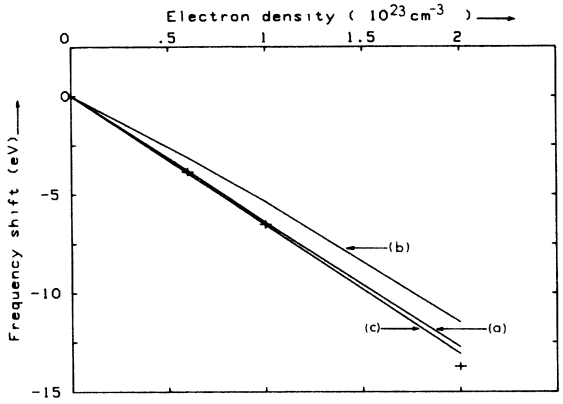

FIG. 4. Density dependence of the Ne X Lyman-γ line shift calculated with $T=500$ eV (same notations as in Fig. 2).

pared with the CASCF line shift (+ + +). In Fig. 2 we report also the Davis and Blaha's[16] red shift (OOO) which is similar to Skupsky's[29] and is 20% smaller than ours. Numerical checks show that this difference comes essentially from the negative contribution by ions. As we have already mentioned, generally the ion gas has not enough time to be effectively polarized ($\tau_i \gg \tau_n$). Therefore the red shift, including the total ion polarization effect, must be considered as the lower limit for the correct one. In Fig. 2, the position of curve (b) which is quite separated from the other ones, shows that the UEGM [numerical solution of Eq. (15) with Eq. (18)] constitutes a poor approximation for treating the $2p$ state at $T=500$ eV. In fact, Fig. 1 shows that the free-electron density is far from uniform in the vicinity of atomic orbits with $n=2$.

Figure 3 represents the density dependence of the Lyman-β red shift and shows once again a good agreement between the QMIT and CASCF results. The same remark is valid for the Lyman-γ red shift illustrated in Fig. 4. However, we note that the UEGM becomes quite reasonable here.

The temperature dependence of the Lyman-α and -β red shift is illustrated in Figs. 5 and 6, respectively. Here we note that the QMIT and CASCF results are similar functions of T and tend towards the UEGM results which are the exact ones when the temperature is high enough to ensure a uniform spatial distribution for free electrons. At intermediate temperatures the good agreement between QMIT and CASCF results can be explained by noting that the first-order perturbation due to monopole-monopole interaction plays a leading part in both of these methods. As shown in Fig. 5, a small discrepancy of about 10% appears at low temperatures where higher-

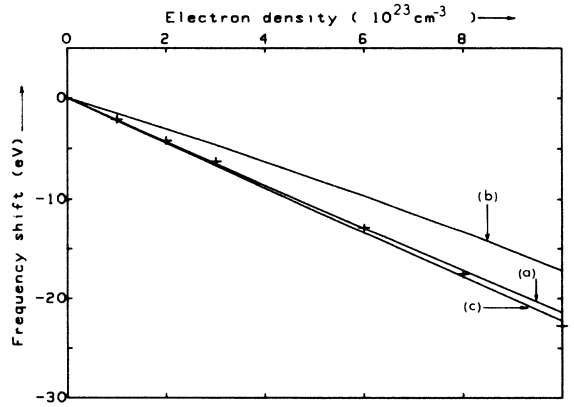

FIG. 3. Density dependence of the Ne X Lyman-β line shift calculated with $T=500$ eV (same notations as in Fig. 2).

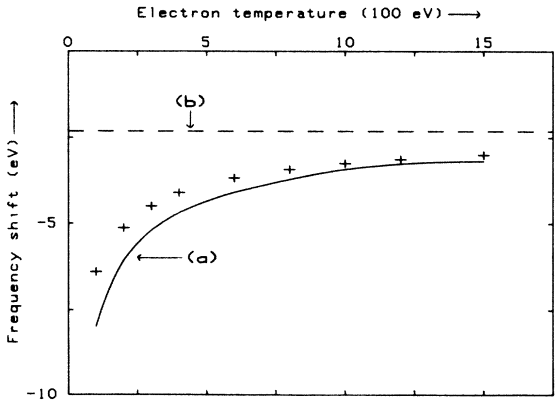

FIG. 5. Temperature dependence of the Ne X Lyman-α line shift calculated with $N_e=10^{24}$ (cm^{-3}). a: quantum mechanical impact theory including the boundary depression effect. b: uniform electron-gas model. + + +: confined atom in self-consistent field.

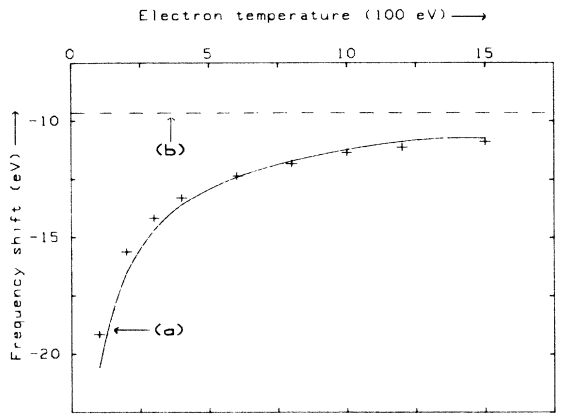

FIG. 6. Temperature dependence of the Ne X Lyman-β line shift calculated with $N_e=6\times10^{23}$ cm^{-3} (same notations as in Fig. 5).

order perturbation terms occur via the unitarized transition matrix, Eq. (23) in QMIT and are included in the CASCF model through the modification of the number density of free electrons, Eq. (5), and the exact solution of the Schrödinger equation, Eq. (15). Also, we must mention exchange effects which have been calculated via the CBO and the local potential approximations in QMIT and CASCF, respectively. Indeed, comparing Figs. 5 and 6 we can see that this discrepancy reduces as exchange effects decrease with increasing principal quantum number n.

We conclude by asserting that the spectral line shift due to electrons in dense and hot plasmas can be obtained either by a correct self-consistent-field method or by a quantum-mechanical line-broadening approach. The former is suitable in giving various important plasma and atomic parameters such as local electron density, density- and temperature-dependent oscillator strengths, while the latter leads to effective atomic lifetimes and enables us to describe conveniently all essential aspects of the binary interaction. To estimate the blue shift due to the ion quadrupolar interaction we can use an expression similar to the second member of Eq. (31) where $D(nl,T)$ should be replaced by a negative ion line-shift coefficient $-Q(n)$. Using Table V of Ref. 30 with fractional widths at $\frac{1}{2}$ intensity points, for example, we obtain $Q(2)=0.8$, $Q(3)=2.1$, and $Q(4)=8.2$ for Lyman-α, Lyman-β, and Lyman-γ line shifts, respectively. Comparing these values with those relative to electrons in Table VI we note that the ion effect consists in reducing the red shift about a few tens of percent. Therefore, the scaling law for spectral line shift, Eq. (31), suggest that radiating ions with small charge Z_E (Ref. 31) are excellent candidates for high-density diagnostics provided that ion-broadening effects[1,2] together with opacity, and spatial-integration[31–35] and time-integration[36] effects are properly taken into account. Our theoretical work in progress concerns principally the inclusion of two and three bound electrons and of relativistic effects for highly charged ions.

ACKNOWLEDGMENTS

We are very grateful to Professor H. Griem for recent helpful discussions at Aussois. This work was supported by Centre National de Recherche Scientifique (CNRS) Grant No. 920052. The Département de Recherchers Physiques is "Laboratoire associé au CNRS No. 040071."

[1]H. G. Griem, M. Blaha, and P. C. Kepple, Phys. Rev. A **19**, 2421 (1979).
[2]H. Nguyen, J. Grumberg, M. Caby, E. Leboucher, and G. Coulaud, Phys. Rev. A **24**, 438 (1981).
[3]H. Nguyen, B. d'Etat, J. Grumberg, M. Caby, E. Leboucher, and G. Coulaud Phys. Rev. A **25**, 891 (1982).
[4]B. d'Etat and H. Nguyen, in the *7th International Conference on Spectral Line Shapes, 1984, Aussois, France,* (de Gruyter, Berlin, 1985).
[5]L. A. Woltz and C. F. Hooper, Jr., Phys. Rev. A **30**, 468 (1984).
[6]H. R. Griem, *Spectral Line Broadening by Plasmas* (Academic, New York, 1974).
[7]P. Jaeglé, G. Jamelot, A. Carillon, A. Klisnick, A. Sureau, and H. Guennou, The 2nd Topical Meeting on Laser Techniques in the Extreme Ultraviolet, 1984, Boulder, Colorado (unpublished).
[8]R. Cauble M. Blaha, and J. Davis, Phys. Rev. A **29**, 3280 (1984).
[9]M. Baus and J. P. Hansen, Phys. Rep. **59**, 1 (1980).
[10]D. R. Inglis and E. Teller, Astrophys. J. **90**, 439 (1939).
[11]R. M. More, J. Quant. Spectrosc. Radiat. Trans. **27**, 345 (1982).
[12]R. Stamm, Y. Botzanowski, V. P. Kaftandjian, and B. Talin, Phys. Rev. Lett. **52**, 2217 (1984).
[13]J. Banon, M. Koenig, and H. Nguyen, Phys. Lett. **101A**, 134 (1984).
[14]H. Nguyen, M. Koenig, and G. Coulaud, Phys. Lett. **106A**, 34 (1984).
[15]M. W. C. Dharma-Wardana and R. Taylor, J. Phys. C **14**, 629 (1981).
[16]J. Davis and M. Blaha, J. Quant. Spectrosc. Radiat. Transfer **27**, 307 (1982).
[17]F. Perrot, Phys. Rev. **20**, 586 (1979).
[18]R. M. More, Phys. Rev. A **19**, 1234 (1979).
[19]B. F. Rozsnyai, Phys. Rev. A **5**, 1137 (1972).
[20]J. B. Stewart and K. D. Pyatt, Jr., Astrophys. J. **144**, 1203 (1966).
[21]M. Baranger, Phys. Rev. **112**, 855 (1958).
[22]O. Bely and H. R. Griem, Phys. Rev. A **1**, 97 (1970).
[23]A. Burgess, D. G. Hummer, and J. A. Tully, Philos. Trans. R. Soc. London **266**, 225 (1970).
[24]M. A. Hayes and M. J. Seaton, J. Phys. B **10**, L573 (1977).
[25]L. B. Golden and D. H. Sampson, J. Phys. B **13**, 2645 (1980).
[26]H. Nguyen, H. W. Drawin, and L. Herman, J. Quant. Spectrosc. Radiat. Transfer **7**, 429 (1967).
[27]Nguyen Hoe and M. Caby, C. R. Acad. Sci. **270**, 1657 (1970).
[28]M. Caby-Eyraud and Nguyen Hoe, J. Phys. B **5**, L153 (1972).

[29]S. Skupsky, Phys. Rev. A **21**, 1316 (1980).
[30]H. R. Griem, Phys. Rev. **27**, 2566 (1983).
[31]P. Lemaire, Thesis, 3rd cycle, University Paris-Sud, Orsay, 1985.
[32]M. J. Herbst and J. Grun, Phys. Fluids **24**, 1917 (1981).
[33]J. C. Gauthier, J. P. Geindre, J. P. Najmabadi, C. Popovics, A. Poquerusse, and M. Weinfeld, J. Phys. D **16**, 1929 (1983).
[34]A. Poquerusse, Opt. Commun. **50**, 364 (1984).
[35]S. Goldsmith, H. R. Griem, and L. Cohen, Phys. Rev. A **30**, 2775 (1984).
[36]R. W. Lee, D. Kilkenny, R. L. Kauffman, and D. L. Mathews, J. Quant. Spectrosc. Radiat. Transfer **31**, 83 (1984).